X-620-70-421
PREPRINT

THE NIMBUS 4 MICHELSON INTERFEROMETER

R. A. HANEL
B. SCHLACHMAN
D. ROGERS
D. VANOUS

DEC. 1970

GSFC
GODDARD SPACE FLIGHT CENTER
GREENBELT, MARYLAND

X-620-70-421
PREPRINT

THE NIMBUS 4 MICHELSON INTERFEROMETER

R. A. Hanel
B. Schlachman
Goddard Space Flight Center

D. Rogers
D. Vanous
Texas Instruments, Inc.

December 1970

Goddard Space Flight Center
Greenbelt, Maryland

THE NIMBUS 4 MICHELSON INTERFEROMETER

ABSTRACT

The Michelson interferometer, IRIS-D, flown on Nimbus 4 in April 1970 is an improved version of the interferometer, IRIS-B, flown on Nimbus 3 a year earlier. Thermal emission spectra of the earth are being recorded between 400 cm^{-1} and 1600 cm^{-1} with a nominal spectral resolution of 2.8 cm^{-1} and a noise equivalent radiance between approximately 0.5 and 1 erg sec^{-1} cm^{-2} $ster^{-1}$ cm. This paper describes the design and performance of the IRIS-D and concentrates on the design differences which exist between the interferometers flown on Nimbus 3 and 4. The performance is demonstrated by examples of spectra obtained while in earth orbit.

CONTENTS

	Page
ABSTRACT	iii
INTRODUCTION	1
INCREASE IN SPECTRAL RESOLUTION	3
SIGNAL-TO-NOISE CONSIDERATIONS	4
ANALOG DATA CHANNEL	6
QUANTIZATION	7
PHASE LOCKED LOOP AND VIBRATION	8
START CONTROL	11
PERFORMANCE OF IRIS-D	11
1. Spectral Responsivity	12
2. Spectral Resolution	13
3. Noise Equivalent Radiance	15
4. Dynamic Range	17
PRELIMINARY RESULTS	17
SUMMARY	18
ACKNOWLEDGEMENTS	19
REFERENCES	20

ILLUSTRATIONS

Figure		Page
1	The infrared interferometer (IRIS-D) on Nimbus 4 consists of an optical module, shown enclosed by a thermal shroud in the center of the figure, and of two modules which contain electronic circuitry. The optical module is mounted below the Nimbus sensory ring (not shown), so that the port visible on top of the shroud views earth. The electronic modules fit into compartments within the sensory ring. The maximum dimension of the shroud across the exposed opening is 44 cm.	22
2	Block diagram of the single sideband phase locked loop which slaves the Michelson mirror motion to the spacecraft clock frequency. Negative feedback using a velocity coil suppresses motor resonances and provides a suitable and stable transfer function of the motor.	23
3	Block diagram of the IRIS-D system. Circuitry to the spacecraft telemetry subsystem to record housekeeping data is omitted.	24
4	Spectral responsivity of IRIS-D during the thermal vacuum test of the spacecraft about 2 months before launch, shortly after the instrument was turned on (orbit 33), and after approximately 5-1/2 months (orbit 2167) of continuous operation in earth's orbit.	25

ILLUSTRATIONS (Continued)

Figure		Page
5	Noise Equivalent Radiance (NER) of IRIS-D calculated from the standard deviation of individual responsivity measurements. The NER curves have been smoothed for display purposes by averaging over 25 cm^{-1}. The NER values obtained while in orbit contain also systematic variations due to orbital temperature changes which will be removed in the final data reduction process.	26
6	Thermal emission spectra recorded by IRIS-D on Nimbus 4. The apodized spectra have a spectral resolution between 2.8 cm^{-1} and 3 cm^{-1}. A hot desert case, an intermediate case over water, and an extremely cold spectrum recorded over the Antarctic are shown. Radiances of blackbodies at several temperatures are superimposed.	27
7	The same spectra as shown in Figure 6 but without apodization. The spectral resolution approaches 2 cm^{-1}. The absorption bands of CO_2, O_3, CH_4 and numerous lines of H_2O can be identified in the spectra. Blackbody temperatures are again shown by dashed lines.	28

INTRODUCTION

The meteorological research satellite Nimbus 4 was launched on April 8, 1970 from the Western Test Range in California into a sun-synchronous, circular, near polar orbit of approximately 1100 km altitude. One of the instruments onboard is a Michelson interferometer, IRIS-D, designed to record the infrared emission spectrum of the earth and its atmosphere between 400 cm^{-1} and 1600 cm^{-1}. The main scientific objective of the IRIS experiment is to use the spectra to derive the vertical profiles of atmospheric temperatures, humidity, and ozone concentrations, for meteorological research as well as to carry out studies of radiative transfer in the atmosphere and of the emissive properties of the earth's surface.

The IRIS-D shown in Figure 1 is an advanced version of the IRIS-B, launched by Nimbus 3 a year earlier, on April 14, 1969. The design and performance of the IRIS-B and scientific results from the Nimbus 3 interferometer experiment have been published (Hanel, et al.[1] 1970; and Hanel and Conrath,[2] 1969; Conrath, et al.[3] 1970; Prabhakara, et al.[4] 1970; Randall and Rawcliffe,[5] 1969). Preliminary results from the Nimbus 4 interferometer experiment have also appeared in print (Hanel and Conrath,[6] 1970). This paper discusses the design and performance of the IRIS-D flown on Nimbus 4. Scientific results from this Nimbus 4 interferometer experiment will be published elsewhere.

The experience gained while testing the IRIS-B model indicated several possible areas where the performance of the instrument might be improved. The original design turned out to be rather conservative in spite of the advancements in the art of infrared emission spectroscopy from space which have been

achieved with this model. Several elements of the IRIS-B were therefore modified for incorporation into IRIS-D.

Probably the most significant change resulted in an increase of the nominal spectral resolution from 5 cm^{-1} to 2.8 cm^{-1}. In spite of the higher resolution it was also possible to improve somewhat on the radiometric precision, particularly noticeable in the region from 1200 to 1600 cm^{-1}, and last but not least, the immunity of the instrument to external vibration was markedly raised.

These improvements were accomplished by a larger displacement of the Michelson mirror, combined with a sacrifice of the 1600 to 2000 cm^{-1} range, by a higher sophistication of the electronic design of the main data channel, and by a redesign of the servo loop which controls the mirror displacement. Several other modifications, such as a positive control of the position of the interferogram peak with respect to the start of an interferogram and careful assembly, alignment, and test procedures may have contributed also to the good performance of the IRIS-D. Except for the modifications mentioned, the interferometers flown on Nimbus 3 and 4 are much alike.

To permit adequate treatment of some of the more interesting points, this paper avoids repetition of information available in the paper on IRIS-B, mentioned above, as much as possible and emphasizes the design changes which distinguish the IRIS-D from its predecessor IRIS-B. For a general discussion of the principles of Fourier spectroscopy, and for further references, the interested reader is referred to surveys on this subject, for example, by J. Connes,[7] 1961; Mertz,[8] 1965; Lowenstein,[9] 1966; Vanasse and Sakai,[10] 1967; and most recently, the

proceedings of the conference on this subject held in Aspen, Colorado in March 1970, to be published by AFCRL.

INCREASF IN SPECTRAL RESOLUTION

The design goal of 5 cm^{-1} wide resolved elements of the IRIS-B was set very early in the program by considerations of the minimum resolution thought necessary for a reasonable atmospheric temperature analysis. At that time 5 cm^{-1} was already a very ambitious goal. Test experience with IRIS-B showed that Michelson interferometers can indeed be made to perform close to their theoretical limits and an increase of the spectral resolution to 2.8 cm^{-1}, even with a conventional thermistor bolometer as an infrared detector, seemed then feasible. From the viewpoint of atmospheric research, higher spectral resolution is definitely desirable.

The resolution increase required several design changes to IRIS-B. First of all, the Michelson mirror had to be moved now 0.36 cm instead of 0.2 cm. Fortunately, the drive motor permitted this without redesign. The single sided action of the IRIS-B motor was converted into a motion symmetrical to the neutral position, thus, the maximum amplitude of the motor displacement was actually reduced. The larger Michelson mirror displacement of IRIS-D required either more sample points per interferogram or a larger separation between them. Both techniques were applied. Without affecting the data format and the interface to the spacecraft, the larger mirror displacement was accomplished by sampling the interferogram every third (1.7557 μ m) instead of every second fringe (1.1705 μm) of the reference interferometer (0.5852 μ m), and by making more efficient use of the permissible number of words within the basic 16

second frame period. Instead of using only 3408 words per interferogram in 10.9 seconds IRIS-D uses 4096 words in 13.1 seconds. A word number equal to a power of two is also more convenient for the Fast Fourier Transform. Furthermore, the upper limit of the spectral range was reduced from 2000 cm^{-1} to 1600 cm^{-1} to permit an adequate and comfortable over-sampling margin. The 1600 to 2000 cm^{-1} range is not essential for reaching the scientific objectives.

The other significant consequence of the resolution increase was a necessary reduction in the field-of-view of the instrument from 4° to 2.5° half cone angle. The reduction of the field-of-view is required to limit the off-axis rays which are increasingly out of phase with respect to the on-axis rays towards the beginning and end of an interferogram. This was accomplished by the use of a smaller thermistor bolometer. The resulting reduction in the field-of-view was also desirable for observational reasons. The circular area under observation during the recording of one interferogram was reduced from a diameter of 150 km to one of 95 km which increased the probability of seeing more homogeneous atmospheric and surface conditions. The interpretation of spectra originating from a homogeneous background is easier and more precise than from spectra where, say, half of the field-of-view is clear and the other half is covered by clouds of different altitudes.

SIGNAL-TO-NOISE CONSIDERATIONS

An increase in spectral resolution necessarily affects also the signal-to-noise and, consequently, the noise-equivalent radiance of the interferometer. The signal-to-noise, S/N, for a spectrometer is (e.g. Hanel,[12] 1970),

$$S/N = \eta_1 \, \eta_2 \, I_\nu \, \Delta\nu \, D^* \, (A \, \Omega \, \Omega_d \, \tau)^{1/2} \qquad (1)$$

By definition, the noise equivalent radiance, NER, is the radiance, I_ν, for which the S/N becomes unity.

$$NER = (\eta_1 \, \eta_2 \, \Delta\nu \, D^*)^{-1} \cdot (A \, \Omega \, \Omega_d \, \tau)^{-1/2} \qquad (2)$$

The systems efficiency, η_1, is 0.35 for single detector interferometers; η_2 is the optical efficiency and $\Delta\nu$ the width of a resolved spectral element. The figure of merit of the detector is D*. A and Ω are the aperture and solid angle of the instrument and Ω_d the solid angle of illumination at the detector. The recording time of the interferogram is τ.

As may be seen from equation (1), the radiant energy available per spectral interval is proportional to $\Delta\nu$ and, therefore, a 5/2.8 fold increase in NER compared to IRIS-B would be expected from this fact alone. Furthermore, the reduction in field-of-view causes another 8/5 increase in NER. If one wanted not only to hold the signal-to-noise ratio at the IRIS-B level, but to improve upon it, if possible, one had to optimize the instrument performance in every conceivable way. All terms of equation (2) were examined for their potential to compensate the desired reduction in $\Delta\nu$ and Ω.

The optical efficiency of the interferometer was raised from about 0.25 to 0.30 primarily by reductions of the optical obscuration. The smaller field-of-view and a careful redesign of some mounts in the path made this possible. A smaller detector (2.3×2.3 mm^2 instead of 3.0×3.0 mm^2) was used which had an effective

D* of 1.02×10^8 cm $Hz^{1/2} w^{-1}$. The smaller solid angle permitted an increase of A from 13 to 15 cm^2 with the same beamsplitter size and, as mentioned before, the recording time, τ, was lengthened from 10.9 to 13.1 seconds. The main improvement, however, came from a redesign of the bolometer bias regulator and preamplifier circuit which permitted a nearly detector-noise-limited operation, as will be discussed in the next paragraph. The theoretically possible NER calculated from the numerical values mentioned above becomes 0.32 cgs units, (erg sec^{-1} cm^{-2} $ster^{-1}$ cm). The actual NER measured during thermal vacuum tests on the spacecraft came within a factor of less than two to the theoretically possible value.

ANALOG DATA CHANNEL

Significant modifications were made to the signal processing electronics to assure, as much as possible, detector noise limited operating conditions. First, the plus and minus 470 volt regulators which supply the bias for the thermistor bolometer and its compensating flake were implemented in an operational amplifier configuration using low noise differential field effect transistors as the input stages. The noise at the 470V bias terminals was about 300nV $Hz^{-1/2}$ absolute and about 90 nV $Hz^{-1/2}$ differential within the band from 5 to 150 Hz. A long term stability of about 10mV was achieved. Secondly, the preamplifier was relocated directly behind the detector. The preamplifier had a gain of 300 and was of thin film hybrid construction using a Field Effect Transistor with a noise voltage of 20nV $Hz^{-1/2}$. By these design changes amplifier and bias supply noise was reduced to about 25% of the detector noise voltage.

Several steps were taken to avoid possible interference from radio frequency sources. The close proximity of the instrument to several spacecraft transmitters was of great concern. The susceptibility of low noise, high gain amplifiers to external fields is known to be high. All leads entering the cavity of the instrument, which houses the detector, were routed through feed-throughs screened for radio frequency interference and all metallic joints were designed to have a gap-to-width ratio that would provide 120 db of attenuation at the radio frequencies present on the Nimbus 4 spacecraft.

The next link in the analog data chain, the band pass filter, was modified also to have a linear phase characteristic. This change was made to minimize the effect of vibration on the instrument data and will be discussed further in the paragraph dealing with that subject.

QUANTIZATION

The increased spectral resolution of IRIS-D compared to IRIS-B resulted in a greater signal-to-noise requirement of about 4000 in the interferogram (this is in the time domain). To accommodate this the number of bits used in the quantization process was increased by one, the automatic scale change factor was reduced from ten to four, and the ratio of quantization increment to rms-noise voltage was slightly raised.

To stably achieve this the analog to digital converter was redesigned using the successive approximation technique. Advantage was taken of the flexibility of this type of converter to simplify the automatic scale change or range standardization system. As a consequence of the additional data bit, the word format had to be slightly modified. The added data bit replaced the parity bit in the IRIS-B

word format. An IRIS-D data word thus consists of two synchronization bits, one gain bit, and nine data bits. The ratio between scales was chosen to have a value of four based on a Fourier analysis of the effective quantization noise produced in the output data spectrum. For the case on hand, the quantization noise produced in the spectrum has a fairly weak minimum for scale factors between 2.5 and 6. The exact value of four was chosen as the most suitable power of two. This ratio was also found convenient in the computer data processing since the gain bit now signals a shift of two positions in the binary word format. The least significant bit magnitude was set equal to twice the rms noise of the signal, leading to a quantization noise in the processed spectra equal to about 20% of the noise produced by the detector and associated electronics, an acceptable value.

PHASE LOCKED LOOP AND VIBRATION

Early in the program the effect of external vibration on the operation of the phase locked loop of the motor drive circuit and on the data quality was investigated. As might be expected, the primary effect of vibration is to cause the moving mirror of the interferometer to oscillate about its required position. At higher levels a secondary effect, misalignment of the interferometer, occurred due to dynamic tilting of the moving mirror support structure. These perturbations of mirror position were shown, both experimentally and analytically, to produce (1) a delay modulation of the interferograms in both the reference and data channels and (2) amplitude modulation of the received power. The latter modulation operating on the total signal occurred at only one frequency, the prime motor resonance at approximately 45 Hz and was noticeable at input levels in

excess of 0.10 g rms measured on the motor housing. This level is well above normal operating conditions. In practice the structural deformation of the moving mirror suspension, or, for that matter, any other part during vibration has not created a problem.

The effect of oscillatory motion of the Michelson mirror around its desired position while the interferometer is exposed to external disturbing forces can be of great importance. Even under phase locked operating conditions a certain amount of delay modulation occurs which is equivalent to phase modulation with differential pre-emphasis. The phase modulation was approximately one radian rms at a vibration input of 0.3 g rms at 45 Hz. In other words, while the design of the phase lock motor drive minimized the deviation, a small residue, the error signal in the loop, is still there and it was considered necessary to prevent distortion being introduced by the electronic low pass filter, provided to eliminate aliasing in the sampling process. This distortion may be eliminated by using a filter with a phase shift linearly proportional to frequency. All frequencies have the same delay then and the shape of the interferogram remains intact. On Nimbus 4 an overall phase characteristic linear to 1° was obtained within the band of interest by using first order all pass phase equalizers in conjunction with third order maximally flat filter sections. Combined with a time delay in the sampling command equal to the time delay in the analog filter the effect of the delay modulation caused by external disturbances can be removed. In the IRIS-D instrument the delay line was not implemented although test results on the breadboard showed the technique to work very well. The circuit was deleted to reduce the complexity of the instrument after the results from

Nimbus 3 indicated lower vibration levels within the spacecraft than originally anticipated. In spite of the rotating solar paddels, tape recorders, and other moving elements, the vibration level in orbit was negligible. This conclusion was derived from inspection of the amplitude of the neon reference signal of IRIS-B in orbit during the flyback portion of the Michelson mirror motion which takes place between interferogram recording and without the phase locked loop operating. Then the interferometer is a very sensitive detector of mechanical vibration. During vacuum thermal testing, for example, the effect of mechanical pumps could easily be seen in the flyback mode while in the operating mode the phase locked loop stabilized the reference interferometer amplitude well.

The design of the Nimbus-D phase locked servo system aimed, among other goals, at a suppression of the effect of the prime motor resonance. The block diagram of the phase locked loop circuits is shown in Figure 2 and an overall block diagram of the instrument in Figure 3. Two items are of interest. First, the use of single sideband translation followed by limiting and phase division to give a wide range (±50 radians) wideband (2 KHz) phase detector, and secondly, similar to IRIS-B, the use of velocity feedback around the motor to obtain a more suitable response, and response stability, for what is effectively a Voltage Controlled Oscillator in the phase locked loop. The advantages that accrued from the use of the wideband extended range phase detector included the acquisition of phase lock from the mirror start position without ever exceeding the range of the phase detector, and the degree to which the servo suppressed the effects of vibration. The first aspect was also significant in maintaining control over the position of the central peak relative to the start and end of an interferogram.

START CONTROL

The data reduction process can be simplified if the position of the center word of the interferogram can be predicted. Servo control of this instrument parameter was incorporated into the IRIS-D design. The ability of the phase locked velocity servo to track the input phase ramp (reference frequency) without ambiguity was combined with an optical position sensor that defined the start position of the moving mirror, and thus the interferogram. The optical position sensor was simple in concept. The shaft of the motor, supporting the movable mirror, passed in front of a slit thus blocking light emitted by a Gallium Arsenide source that normally illuminated a silicon photo-diode. This transducer under the control of the instrument sequencer was used to set the initial conditions of the phase locked servo. Nonlinear analysis techniques, such as the phase-plane method, were used to ensure that stability problems would not occur. A fail-safe approach was taken in that the light emitted was checked during operation and, if a failure of the light source should have occurred, the system would have reverted to the operating mode of IRIS-B where the center position was not controlled actively. The center word control circuit has worked well in orbit. The measured variance of the central peak position from the predicted value is 0.6 words, or about one micrometer.

PERFORMANCE OF IRIS-D

The performance of a spectrometer can be described by certain characteristic parameters. Most commonly used are the spectral responsivity, the spectral resolution, the noise equivalent radiance and the dynamic range of the instrument. Additional parameters, such as wave number calibration, instrument function,

field-of-view, as well as the stability of all the parameters with temperature and time, are also significant. Test data, as well as data obtained by the instrument while in orbit, serve to establish the parameters just mentioned. Some parameters could be determined with high precision, others are less well-defined. In some cases the work is still incomplete and will be reported elsewhere.

1. Spectral Responsivity

The responsivity of IRIS is defined by the equation

$$C(\nu) = r(\nu)\,[I(\nu) - I_i(\nu)] \tag{3}$$

The spectral amplitude, $C(\nu)$, is the number of digits (zero to peak) of a particular frequency component in the interferogram divided by the maximum number of digits within the dynamic range of the quantizing circuits. Normalization of the spectral counts to the maximum quantization level permits comparison of instruments with different quantization arrangements. $I(\nu)$ is the radiance of the observed scene and $I_i(\nu)$ the radiance of the instrument. With the help of two calibration blackbodies the responsivity may be calculated without a knowledge of the instrument radiance which is more difficult to determine in view of small temperature gradients within the interferometer.

$$r(\nu) = [C_w(\nu) - C_c(\nu)]\,[B_w(\nu) - B_c(\nu)]^{-1} \tag{4}$$

B_w and B_c are the Planck functions corresponding to the warm and cold calibration blackbodies.

During tests of the instrument in vacuum chambers the cold blackbody was usually at liquid nitrogen temperature while in orbit the interstellar space served

as reference. It was considered to be a perfect radiation sink, $B_c = 0$. For ground testing and in orbit the built-in blackbody at about 285°K served as the warm reference source. This temperature was monitored by a platinum wire element to 0.2°K. The responsivities measured in the spacecraft systems test, about two months before launch, and in orbit shortly after launch as well as after about five and one half months in orbit are shown in Figure 4.

Most gratifying was the optical-mechanical stability of the instrument as manifested by the constancy of the responsivity between the prelaunch tests and while in orbit. Without requiring realignment the interferometer survived vibration and vacuum testing on the ground, shipments, and finally the launch on a Thor Agena rocket.

The low wave number cutoff of 400 cm^{-1} (25 μ) of the responsivity is caused by potassium bromide, the beamsplitter substrate material. At the upper design limit, 1600 cm^{-1}, the responsivity is still acceptable. Beamsplitter coatings, entrance window transmission, and thermistor bolometer response determine the detail shape of the curve.

2. Spectral Resolution

The nominal spectral resolution of a Michelson interferometer is generally defined by (e.g., Vanasse and Sakai,[10] 1967)

$$\Delta\nu = \frac{1}{2\,\delta_{max}} \tag{5}$$

The resolving power

$$R = \frac{\lambda}{\Delta\lambda} = \frac{\nu}{\Delta\nu} = \frac{\delta_{max}}{\lambda/2} \tag{6}$$

becomes equal to the number of half wavelength which fall into the space from zero to δ_{max}. In practice it is often difficult to define the zero path difference point in the interferogram, particularly for interferometers which cover a wide spectral range, as in the case of IRIS. The zero path difference point is slightly wavenumber dependent primarily due to dispersion in the beamsplitter substrate material and, consequently, the interferogram is not perfectly symmetrical. Therefore, the IRIS was designed to record the interferogram from $-\delta_{max}$ to $+\delta_{max}$. It is well known that no gain in spectral resolution can be realized, but some gain in signal-to-noise ratios ($\sqrt{2}$) and freedom from the zero path difference problem is achieved.

Applying the resolution criterion to IRIS-D which has a mechanical displacement of the Michelson mirror of 0.36 cm and, consequently, an optical displacement of 0.72 cm from $-\delta_{max}$ to $+\delta_{max}$ yields a nominal spectral resolution of 1.4 cm^{-1}. This resolution corresponds to the unapodized mode of data reduction and is not expected to be fully realized due to the natural apodizing effect of the off-axis rays. Judging from the width of the Q-branch of CO_2 at 667 cm^{-1}, quite apparent in all test spectra taken in air, the actual resolution of the unapodized spectra is closer to 1.8 cm^{-1}, taking into account the finite width of the Q-branch at atmospheric pressure. Preliminary estimates from atmospheric spectra seem to confirm an unapodized resolution close to 2 cm^{-1} near 1000 cm^{-1} and probably closer to 2.5 cm^{-1} at the higher wavenumber end of the spectrum.

In the apodized mode of data reduction the nominal spectral resolution of IRIS-D is 2.8 cm^{-1} and in reality probably closer to 3 cm^{-1}. More precise determinations are in progress, as well as estimates on the wavenumber accuracy.

3. Noise Equivalent Radiance

A measurement of an unknown physical quality is really useless unless an estimate of the probable error is made also. One has to distinguish between the precision of a measurement and the accuracy. The precision of IRIS-D is estimated from the repeatability of measurements made under the same conditions. A determination of the absolute accuracy is more difficult and is made by determining the temperature of a blackbody which temperature is sensed also by other means.

The noise equivalent radiance, NER, expressed the repeatability of the measurements in radiometric terms and permits, therefore, a comparison of instruments of different designs. The NER is the sample standard deviation, s, within the measured spectra recorded while observing a particular scene constant with respect to time. The NER is calculated for each spectral interval resolved.

$$\mathrm{NER}\ (\nu) = s\ [I\ (\nu)] \tag{7}$$

The spectral radiance, I, of an unknown source is derived from

$$I = (C_t - \bar{C}_c)\ (\bar{C}_w - \bar{C}_c)^{-1}\ B_w \tag{8}$$

where C_t, C_w, C_c are the spectral amplitudes recorded while observing the source, a warm (B_w) and a cold ($B_c = 0$) calibration blackbody, respectively. All quantities depend on ν. Many calibration spectra are averaged so that the random fluctuations of I are primarily caused by the fluctuations in the C_t, derived from a single interferogram, and, therefore,

$$\mathrm{NER} = s\ (C_t)\ B_w\ (C_w - \bar{C}_c)^{-1} = s\ (C_t)\ \bar{r}^{-1} \tag{9}$$

It is also possible to derive NER from the calibration spectra by operating with the responsivity calculated from individual pairs of warm and cold calibration spectra with the help of

$$s(r) = [s^2(C_w) + s^2(C_c)]^{1/2} \bar{B}_w^{-1} \tag{10}$$

and assuming that the random fluctuations are the same for both calibration spectra, the NER may also be calculated from

$$NER = s(r) B_w 2^{-1/2} \bar{r}^{-1} \tag{11}$$

Only this equation was used for orbital conditions while both methods have been used in ground testing. In some earlier communications the square root of two was erroneously omitted.

The NER derived from thermal vacuum test of the spacecraft are shown in Figure 5 along with results obtained in orbit. To permit a more suitable display, the values shown in Figure 5 are the running averages over 25 wavenumbers. Without smoothing the individual curves would strongly overlap. Each curve is calculated from the calibration pairs from one orbit which are about 18 cold and 18 warm blackbody spectra. The orbital values contain not only the random variations in the responsivity but also a certain amount of systematic variations caused by small temperature changes within the instrument over the period of one orbit. The effect of these changes will be removed in the final data reduction process. The final NER caused primarily by the statistical fluctuations in the system is expected to be somewhat smaller than the values shown in Figure 5. IRIS had electrical power applied in orbit 21 and at orbit 33 the instrument had not yet equalized completely, which might explain the somewhat higher NER in that orbit.

4. Dynamic Range

The dynamic range of the spectrometer has been chosen to cover a wide range of radiances from zero to that of a blackbody of about 300°K. Of course, the brightness temperature of individual spectral intervals may exceed 300°K such as has occurred while observing desert regions but in the spectral average the radiance must be below that of a blackbody of 300°K. This dynamic range was found to be adequate to cope with all conditions on earth; so far saturation of the analog to digital converter has not occurred.

PRELIMINARY RESULTS

The spectra shown in this paper should be considered preliminary. Several refinements in the calibration procedure are being implemented into the final reduction process. These refinements include a recognition of the orbital temperature changes of the instrument and some deviations from ideal blackness of the calibration blackbody. All these effects are small and will hardly be noticeable in the graphical presentation of the spectra at the scale of journal reproductions, but they may be significant for the numerical interpretation tasks for which the IRIS spectra are intended.

Typical emission spectra recorded by IRIS on Nimbus 4 are shown in Figure 6 and Figure 7. The apodization function applied to the interferograms which yielded the spectra shown in Figure 6 is identical to the one applied to the Nimbus 3 data, discussed previously, $(0.54 + 0.46 \cos 2\pi\tau/T)$. The spectra of Figure 7 are the same as shown in Figure 6 but without apodization applied. An extremely warm and a cold spectrum, as well as an intermediate case, have been chosen for demonstration purposes. The spectral features are caused

predominantly by CO_2, H_2O, and O_3 absorption and remission. Near 1300 cm^{-1} CH_4 and N_2O contribute also to the structure. The radiance at certain strategically located spectral intervals serves to derive the vertical profiles of temperature, humidity, and ozone as discussed, for example, in the papers on the scientific results of the Nimbus 3 interferometer experiment.

As discussed previously, the Sahara spectrum shows again a reststrahlen feature between 1000 and 1200 cm^{-1} attributed to SiO_2 in the desert sand. A further discussion of the same spectra is given elsewhere (Hanel and Conrath,[6] 1970).

SUMMARY

The interferometer (IRIS-D) flown on Nimbus 4 in April 1970 is an improved version of the instrument (IRIS-B) flown on Nimbus 3 a year earlier. The main improvements resulted in an increase in spectral resolution to 2.8 cm^{-1}, a reduction in the field-of-view to 2.5 degrees half cone angle, a noise equivalent radiance of less than 1 cgs unit over most of the spectral range which is from about 400 cm^{-1} to 1600 cm^{-1}. A higher immunity of the instrument to external vibration and to radio frequency interference was also achieved. The performance of the instrument has been demonstrated by examples of test results and of preliminary spectra obtained while in orbit. Combined with a long lifetime of Nimbus 4 a unique set of data is being accumulated which is expected to be valuable for many tasks in the art of remotely sensing atmospheric and surface conditions. Primarily meteorology, but other areas of applied science will benefit. The obtained spectra are a vivid demonstration of the potential of Fourier spectroscopy for the exploration of planetary atmospheres and surfaces, including those of the planet we happen to live on.

ACKNOWLEDGEMENTS

The authors are grateful to C. Kruger and M. Rhodes of Texas Instruments for their invaluable assistance in the development of the IRIS-D instrument and to G. Wolfard of GSFC for his efforts in the area of data reduction. Mr. Milton Sing, GSFC, helped in the preparations of the figures.

REFERENCES

1. R. A. Hanel, B. Schlachman, F. D. Clark, C. H. Probesh, J. B. Taylor, W. M. Wilson, and L. Chaney, Appl. Opt. 9, 8, 1767 (1970).

2. R. A. Hanel and B. J. Conrath, Science 165, 1258 (1969).

3. B. J. Conrath, R. A. Hanel, V. G. Kunde, and C. Prabhakara, J. Geophys. Res. Oceans and Atmospheres, 75, 30, 5831 (1970).

4. C. Prabhakara, B. J. Conrath, R. A. Hanel and E. J. Williamson, Journal of Atmosph. Sciences, 27, 4, 689 (1970).

5. C. M. Randall and R. D. Rawcliffe, Proceedings of the Society of Photo-Optical Instrumentation Engineers, 15th Technical Symposium, Sept. 14-17, 1970, Anaheim, Calif.

6. R. A. Hanel and B. J. Conrath, Nature, 228, No. 5267, 143 Oct. 10 (1970).

7. J. Connes, Rev. Opt. 40, 45, 116, 171, 231 (1961).

8. L. Mertz, Transformations in Optics (Wiley, New York, 1965).

9. E. V. Loewenstein, Appl. Opt. 5, 5, 845 (1966).

10. G. Vanasse and H. Sakai, Progress in Optics, E. Wolf, Ed. (North-Holland Publ. Co., Amsterdam, 1967), Vol. 6.

11. "1970 International Conference on Fourier Spectroscopy," to be published by Air Force Cambridge Research Laboratory (in press).

12. R. A. Hanel, in Advances in Geophysics, H. E. Landsberg and J. Van Mieghem, Eds. (Academic Press Inc., New York, 1970), Vol. 14, Chap. 13 (A. J. Drummond, Ed.).

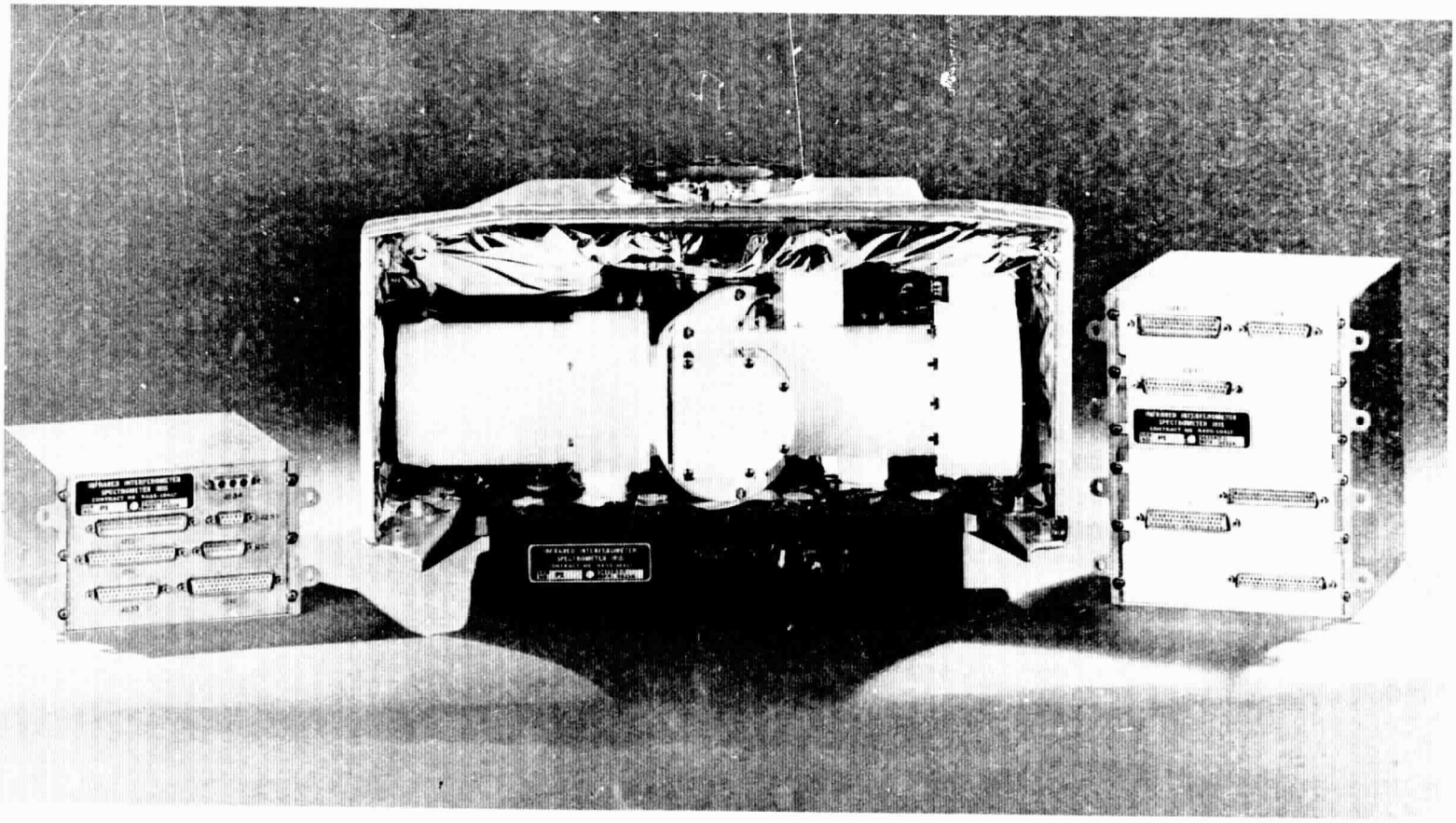

Figure 1. The infrared interferometer (IRIS-D) on Nimbus 4 consists of an optical module, shown enclosed by a thermal shroud in the center of the figure, and of two modules which contain electronic circuitry. The optical module is mounted below the Nimbus sensory ring (not shown), so that the port visible on top of the shroud views earth. The electronic modules fit into compartments within the sensory ring. The maximum dimension of the shroud across the exposed opening is 44 cm.

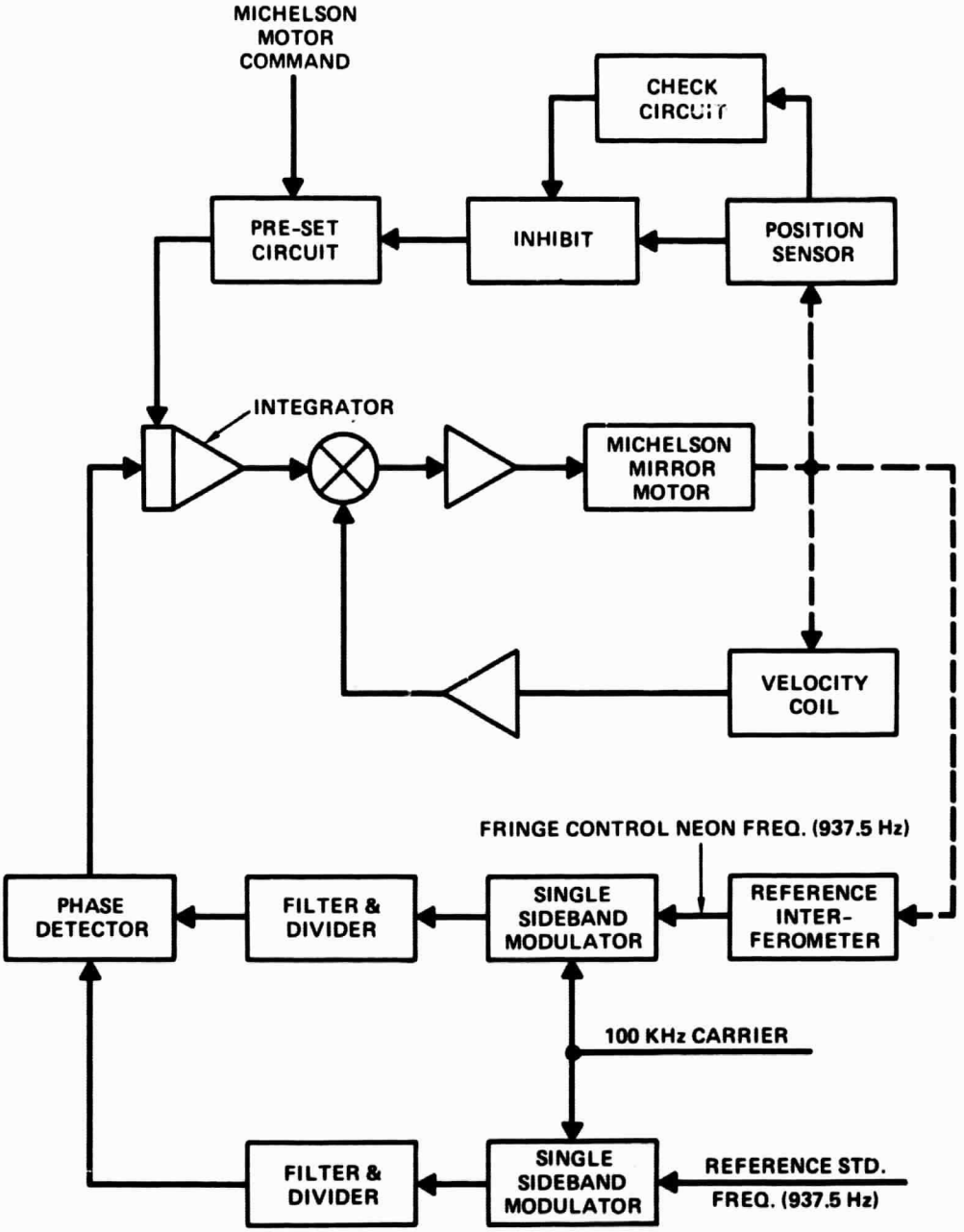

Figure 2. Block diagram of the single sideband phase locked loop which slaves the Michelson mirror motion to the spacecraft clock frequency. Negative feedback using a velocity coil suppresses motor resonances and provides a suitable and stable transfer function of the motor.

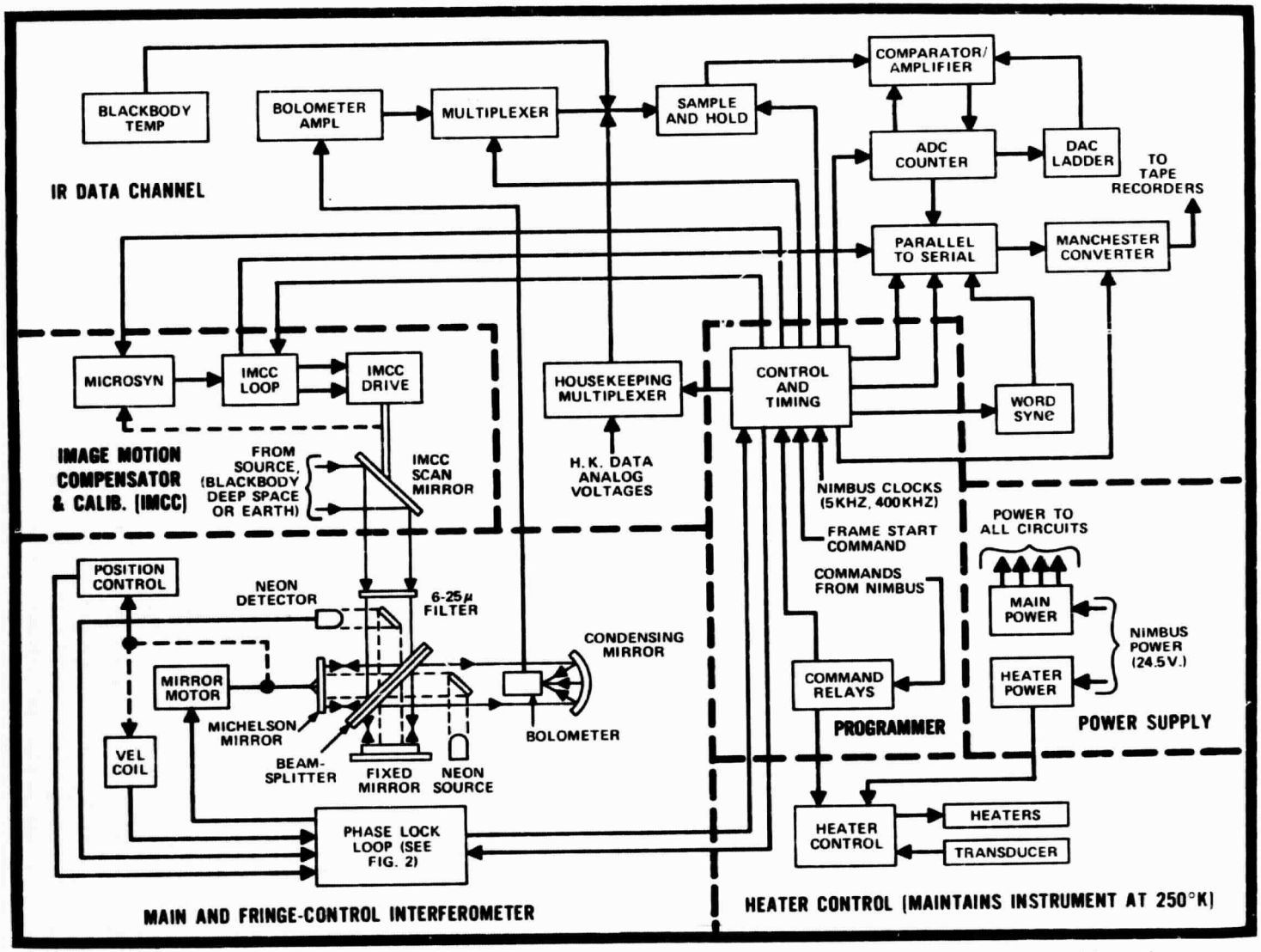

Figure 3. Block diagram of the IRIS-D system. Circuitry to the spacecraft telemetry subsystem to record housekeeping data is omitted.

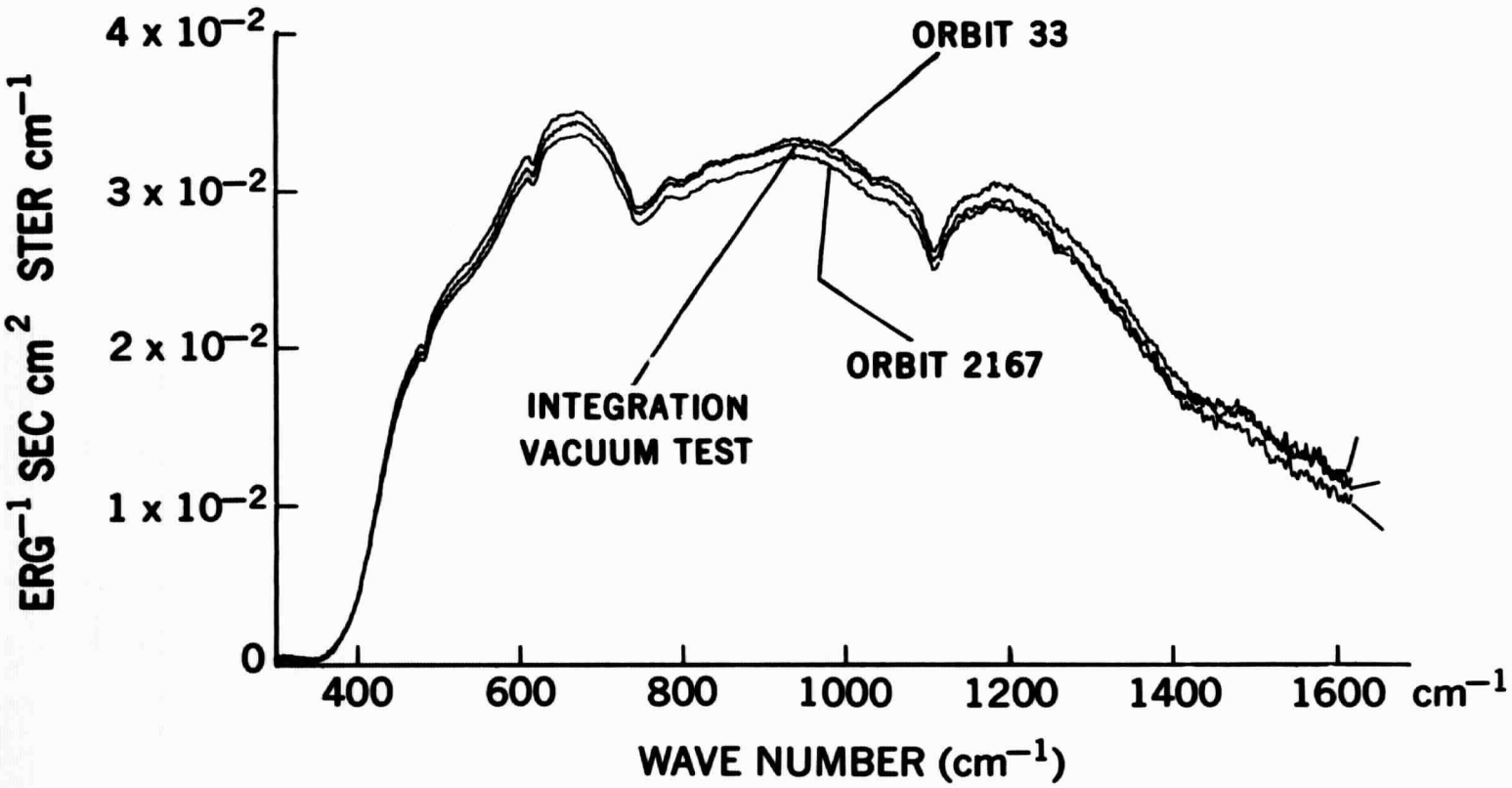

Figure 4. Spectral responsivity of IRIS-D during the thermal vacuum test of the spacecraft about 2 months before launch, shortly after the instrument was turned on (orbit 33), and after approximately 5-1/2 months (orbit 2167) of continuous operation in earth's orbit.

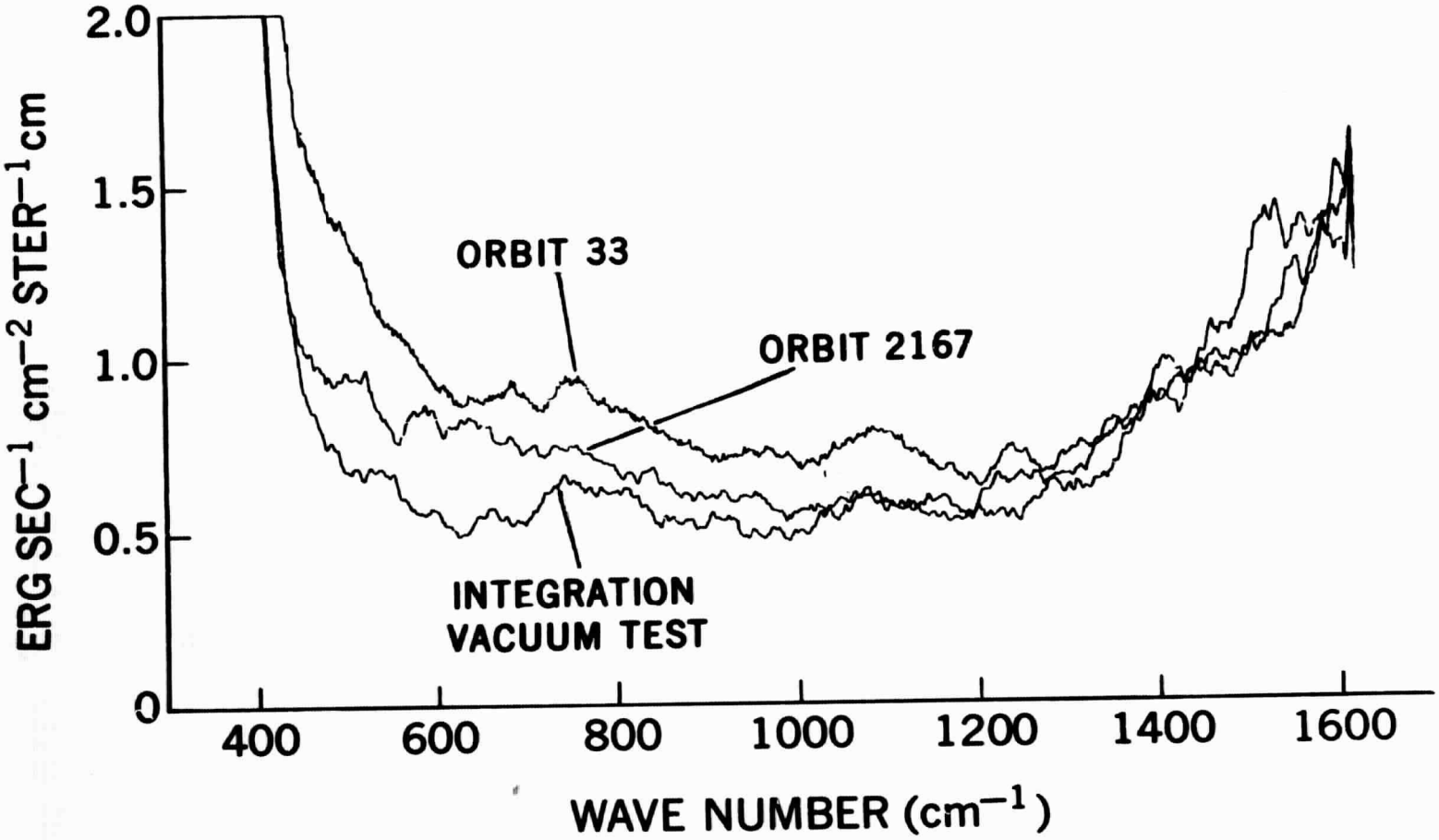

Figure 5. Noise Equivalent Radiance (NER) of IRIS-D calculated from the standard deviation of individual responsivity measurements. The NER curves have been smoothed for display purposes by averaging over 25 cm^{-1}. The NER values obtained while in orbit contain also systematic variations due to orbital temperature changes which will be removed in the final data reduction process.

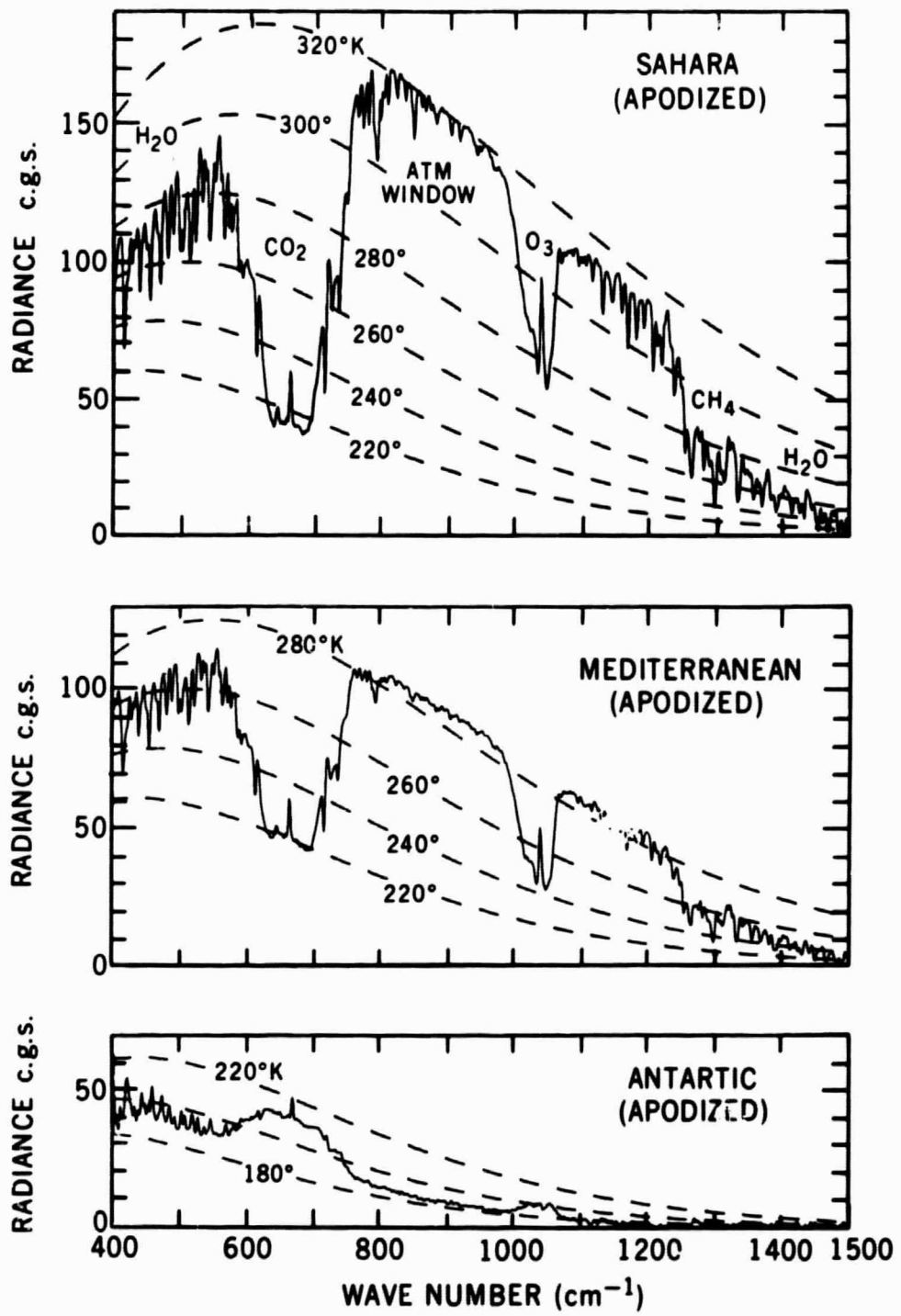

Figure 6. Thermal emission spectra recorded by IRIS-D on Nimbus 4. The apodized spectra have a spectral resolution between 2.8 cm^{-1} and 3 cm^{-1}. A hot desert case, an intermediate case over water, and an extremely cold spectrum recorded over the Antarctic are shown. Radiances of blackbodies at several temperatures are superimposed.

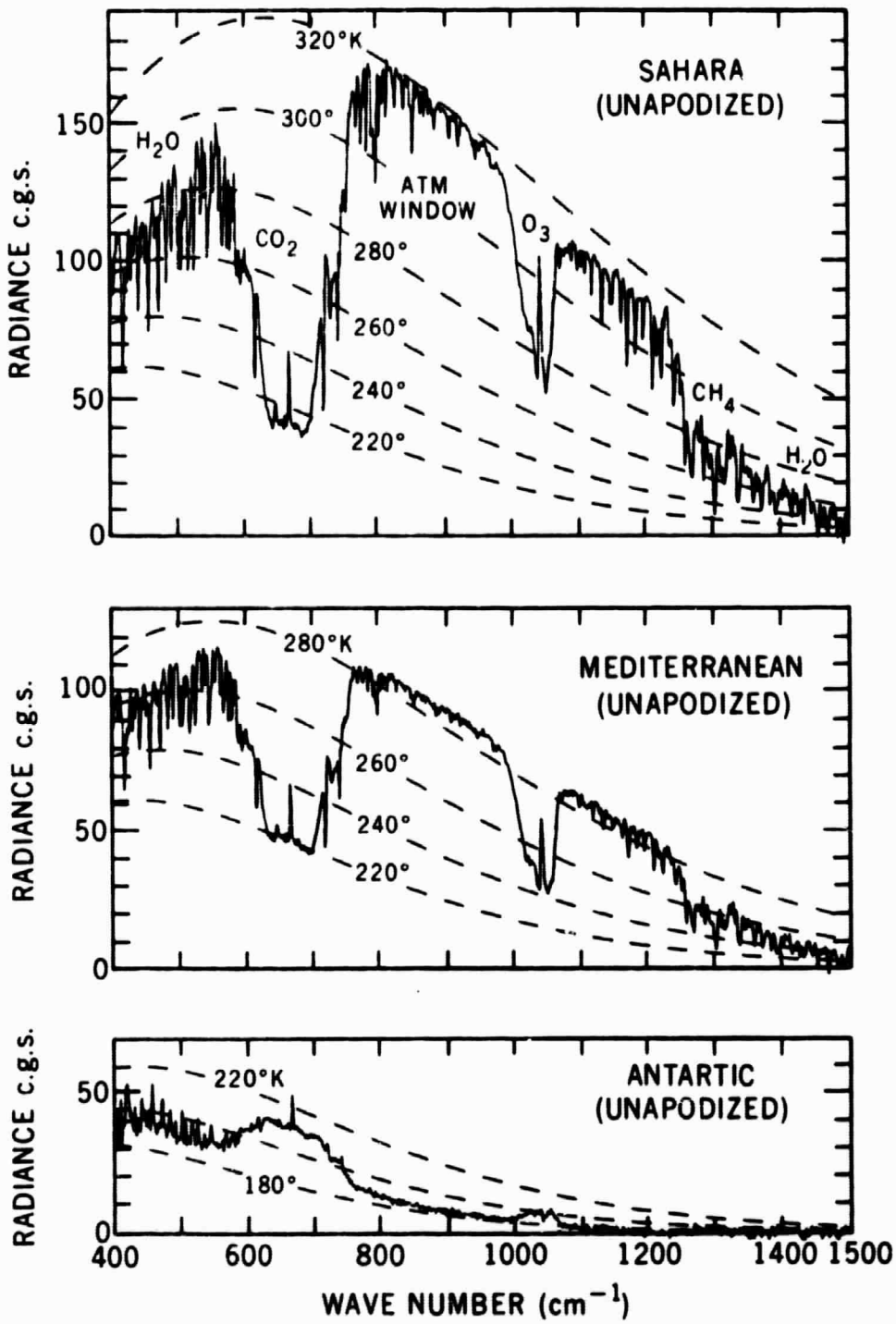

Figure 7. The same spectra as shown in Figure 6 but without apodization. The spectral resolution approaches 2 cm^{-1}. The absorption bands of CO_2, O_3, CH_4 and numerous lines of H_2O can be identified in the spectra. Blackbody temperatures are again shown by dashed lines.